Contract No.:

This manuscript has been authored by Battelle Savannah River Alliance (BSRA), LLC under Contract No. 89303321CEM000080 with the U.S. Department of Energy (DOE) Office of Environmental Management (EM).

Probing the Thermal Decomposition of Plutonium (III) Oxalate with IR and Raman Spectroscopy, X-ray Diffraction, and Electron Microscopy

Jonathan H. Christian,[a,b] Bryan J. Foley,[a] Elodia Ciprian,[b] Jason Darvin,[c] Don D. Dick,[c] Amy E. Hixon,[b*] Eliel Villa-Aleman[c*]

[a] Chemical Processing Section, Savannah River National Laboratory, Aiken, SC 29808 USA
[b] Department of Civil & Environmental Engineering & Earth Sciences, University of Notre Dame, Notre Dame, IN, 46556 USA
[c] Nuclear Nonproliferation Division, Savannah River National Laboratory, Aiken, SC 29808 USA

*Corresponding Authors:
Eliel.Villa-Aleman@srnl.doe.gov
ahixon@nd.edu

Abstract
The thermal decomposition of Pu(III) oxalate was analyzed by Raman microspectroscopy, infrared spectroscopy, scanning electron microscopy, and powder X-ray diffraction. These data show that crystalline $Pu_2(C_2O_4)_3 \bullet 9H_2O$ progressively loses water and oxalate ligands as it is heated, which leads to a decrease in long-range lattice ordering, though minimal changes are observed in gross crystalline morphology. The onset of PuO_2 formation was observed between 200 - 250 °C. Thermal decomposition of oxalate ligands leads to the formation of CO_2 and plutonium oxalate-carbonate moieties, which had not been observed in previously published thermogravimetric measurements of Pu(III) oxalate. Formation of plutonium oxalate-carbonate moieties is believed to be associated with a change in the plutonium oxidation state from 3+ to 4+, which occurs prior to PuO_2 formation. The data provided herein demonstrate the rich spectroscopic nature of a rather underexplored, and technologically relevant, plutonium system. Ideally these results will further future investigations into the Pu(III) oxalate system both experimentally and computationally.

Keywords: plutonium oxalate, plutonium dioxide, thermal degradation, calcination, nonproliferation, nuclear forensics

1. Introduction

Plutonium oxalate solids are routinely calcined to produce PuO_2. The production of PuO_2 from Pu oxalate - commonly referred to as the "plutonium oxalate method"- is the standard processing method for plutonium at industrial-scale fuel and waste reprocessing facilities.[1-3] Although the plutonium oxalate method has been utilized extensively for over 80 years, the mechanism of thermal decomposition remains uncertain, as summarized in several recent reports.[1, 4-6]

To date, most studies aimed at understanding the decomposition mechanism of Pu oxalate have focused on Pu(IV) oxalate. In fact, there are at least nine different reports in the literature that have studied the thermal decomposition of Pu(IV) oxalate.[5, 7-14] While most of these reports have demonstrated similar results, subtle differences have been reported using different analytical techniques, including thermogravimetric analysis (TGA), powder X-ray diffraction (pXRD), and vibrational spectroscopy. Far fewer reports have been published on the thermal decomposition of Pu(III) oxalate, and to date, the thermal decomposition mechanism of Pu(III) oxalate has only been assessed using TGA.[15] Given the prevalence and utility of Pu(III) oxalate in the nuclear fuel cycle, the lack of spectroscopic, microscopic, and X-ray analyses to support chemical assignments during the thermal decomposition of Pu(III) oxalate is a clear deficiency.

Vibrational spectroscopy is a particularly useful tool for identifying chemical composition and structural transformations in Pu-bearing compounds, including PuO_2 and Pu oxalate,[5, 16-22] yet only two studies to date have utilized vibrational spectroscopy to study Pu(III) oxalate.[6, 23] In 2021, Corbey et al. published a comprehensive series of time-resolved pXRD measurements coupled with solid-state optical spectroscopy and electron microscopy to evaluate the auto-decomposition of both Pu(III) and Pu(IV) oxalate as they aged in air.[6] This study showed that both Pu(III) and Pu(IV) oxalate produce rich infrared spectra that can be used to track auto-decomposition due to radiolysis. In 2015, Tamain et al. published the Raman spectrum of a Pu(III) oxalate compound, $Pu_2(C_2O_4)_3(H_2O)_6 \bullet 3(H_2O)$ *[i.e., $Pu_2(C_2O_4)_3 \bullet 9(H_2O)$]* which provided an exquisite look at the structural features of hydrated Pu(III) oxalate for the first time.[23]

Given the wealth of chemical and structural information that can be measured for Pu oxalate using vibrational spectroscopy, our group recently published an in-depth look at the thermal decomposition mechanism of Pu(IV) oxalate using IR and Raman spectroscopy, with ancillary pXRD

and scanning electron microscopy (SEM) measurements, as well as density functional theory analysis.[5, 24] Our results elucidated the decomposition mechanism of Pu(IV) oxalate in a way that was never done before, providing far greater detail than TGA measurements alone, particularly with regards to the structural moieties and crystalline morphologies produced during the decomposition.

In this report, we study the thermal decomposition of hydrated Pu(III) oxalate nonahydrate, $Pu_2(C_2O_4)_3 \bullet 9H_2O$, as it is heated in air up to 450 °C. Using a combination of IR and Raman spectroscopy, pXRD, and SEM, the thermal decomposition of Pu(III) oxalate is presented in detail. The spectroscopic signatures identified herein can be leveraged in applied nuclear forensics and nonproliferation campaigns, and the vibrational modes identified in this study can be used to validate computational models that describe the chemical structure of Pu(III) oxalate and its thermal decomposition products. Together, these results are of fundamental importance towards better understanding the plutonium fuel cycle and advancing nuclear nonproliferation goals by creating a catalog of plutonium-based spectroscopic signatures which should enable rapid, high-resolution chemical identification of obtained materials.

2. Experimental Methods

2.1 Plutonium (III) oxalate preparation

All plutonium syntheses were performed inside of negative pressure radiological gloveboxes that permit the safe handling of weapons-grade plutonium (> 93 % ^{239}Pu).

Plutonium nitrate (1 mL; 0.0975 M in HNO_3; 0.0975 mmol Pu) was added in one portion to a stirring solution of L-ascorbic acid (36 mg in 500 µL of deionized water; 0.20 mmol; 2.09 eq.) in a 20 mL scintillation vial. The solution immediately became royal blue upon the addition of the plutonium solution. After 30 minutes of stirring, a solution of oxalic acid dihydrate (29 mg in 360 µL deionized water; 0.23 mmol; 2.4 eq) was added to the reaction vessel in two portions over 30 minutes (note, the excess of oxalic acid here was important to afford efficient precipitation). After stirring for an additional 20 minutes, the solution afforded a blue precipitate and a colorless supernatant. These solids were vacuum filtered through a PVDF membrane in a plastic filtration apparatus. The solids were washed several times with deionized water. Upon retrieval, 40.4 mg of teal solids were obtained which corresponds to a 92% isolated yield assuming the formula $Pu_2(C_2O_4)_3 \bullet 9(H_2O)$

A small amount of these solids was set aside. The remaining solids were portioned into separate quartz crucibles for calcination. All crucibles were placed into a muffle furnace together at the same time. The temperature of the furnace was then increased to the lowest desired temperature. After one hour of heating at the desired temperature, a crucible was removed, and the oven temperature was increased to the second desired temperature. After one hour of heating at the second temperature, a second crucible was removed, and the temperature of the oven was set to the third desired temperature, and so on. A total of five samples were heated in this manner at temperatures of 160, 200, 250, 300, and 450 °C. The temperatures selected were based on previously-reported thermogravimetric analysis data that indicated significant mass changes occur near these temperatures due to dehydration of Pu(III) oxalate, followed by oxidation to PuO_2.[15] Hereafter, these solids are referred to as **Pu-X** with **X** indicating the maximum temperature at which the solid had been heated. Thus, for the solids that were not heated and were set aside immediately after ambient temperature filtration, they are labeled **Pu-25**. Similarly, solids heated up to 450 °C are labeled **Pu-450**.

2.2 Spectroscopy Sample Preparation

Solid samples were spotted onto a piece of carbon tape within a patent-pending containment cell. The cell was sealed under an argon environment. All characterization measurements were acquired within one week of sample production to limit the degree of lattice damage due to alpha-radiolysis or moisture uptake.

2.3 Raman Spectroscopy

A LabRAM HR800 UV (Horiba Jobin-Yvon) high-resolution confocal μ-Raman spectrometer equipped with an iDus charge-coupled device (CCD) detector (Andor DU416A-LDC-DD) with a 2000 × 256 pixel array and 15-μm pixel resolution was used to acquire Raman spectra. The detector was cooled to -92 °C using a water chiller and a binning of 2 was used for most experiments. A 514 nm laser was as the excitation source with a power of 250 μW at the sample window to avoid heating samples. The laser power was controlled using a combination of half waveplate and polarizer while monitoring the laser power at the exit of the 50x objective used to focus light onto the sample. The exciting laser light was eliminated from the back-reflected light from the sample by using an ultra-steep, long pass edge filters acquired from Semrock Inc. to enable interrogation the vibrational spectra within 50 cm^{-1} of the laser excitation line. A 1800 g/mm grating in the visible range was used to disperse light incident onto the detector. Data acquisition was controlled using Labspec 5.78 software with an acquisition time varying from few minutes to several hours to obtain a high signal to noise ratio for each sample. This software was also used to remove cosmic rays by co-adding at least 2 spectra and was also used to process the acquired data. Raman spectra presented in this manuscript are the average of multiple spectra (up to 10) which were acquired by interrogating different regions of the sample to ensure reproducibility.

2.4 Infrared Spectroscopy

A Nicolet 6700 spectrometer and a microscope was used to measure diffuse reflectance infrared Fourier transform spectroscopy (DRIFTS). A liquid nitrogen cooled mercury cadmium telluride (MCT) detector was used to record spectral measurements. Spectra had a 4 cm^{-1} resolution and were recorded in the 800 cm^{-1} - 5500 cm^{-1} spectral window. Infrared transmission measurements below 800 cm^{-1} were limited by the BaF_2 windows used in our patent pending double walled spectroscopy cells. A single data acquisition period averaged 2000 individual spectra. Baseline removal was performed in Origin Pro software. Multiple measurements were performed on each sample to confirm reproducibility.

2.5 Powder X-ray Diffraction

A single crystal X-ray diffractometer (SC-XRD) was used to acquire powder X-ray diffraction (pXRD) data. Less than 1 mg of each sample was mounted on the end of a glass fiber using epoxy and measured on a Rigaku XtaLab Synergy-S SC-XRD with monochromated Cu-Kα radiation (**Pu-25**, **Pu-250**, **Pu-300**, and **Pu-450**) or a Bruker Quazar SC-XRD with monochromated Mo-Kα radiation (**Pu-160** and **Pu-200**), as described elsewhere.[25] To allow for direct comparison, all patterns

were converted to Cu-Kα 2θ values and phase determinations were completed using the International Centre for Diffraction Data (ICDD) database.[25]

2.6 Scanning Electron Microscopy

The morphology of plutonium(III) oxalate and its thermal degradation products was observed using a JEOL JCM-6000 Plus Benchtop scanning electron microscope operating at 15 kV in secondary electron (SE) mode at magnifications between 1000x and 5000x. All samples were mounted on carbon tape adhered to an aluminum stub and were prepared inside a glovebox. The lexicon developed by Tamasi et al.[26] was used to consistently describe the qualitative nature of each sample, as indicated by the italicized text in section 3.2.

3. Results

3.1 Powder X-ray Diffraction (pXRD)

pXRD measurements of the blue solids of **Pu-25** (Fig. 1 and Fig. S1) are consistent with $Pu_2(C_2O_4)_3$•$9(H_2O)$, as shown by the close match of the experimental pattern to the published powder diffraction file for $Pu_2(C_2O_4)_3$•$9(H_2O)$ (PDF #04-016-7987).[26] This result is consistent with TGA data reported by De Almeida et al., which show that Pu(III) oxalate nonahydrate is the favored form of Pu(III) oxalate formed by precipitation in air at room temperature.[15]

Once heated, noticeable color changes were observed for the Pu solids. The color changed from turquoise to brown and then dark green/black along the progression of temperatures from **Pu-25** to **Pu-450**. As shown in Fig. 1, pXRD measurements of **Pu-160** and **Pu-200** resulted in amorphous diffraction patterns that could not be assigned to a specific compound. According to the TGA measurements of De Almeida et al., dehydration from $Pu_2(C_2O_4)_3$•$2(H_2O)$ to $Pu_2(C_2O_4)_3$•(H_2O) occurs between 140 °C and 180 °C, and dehydration from $Pu_2(C_2O_4)_3$•(H_2O) to $Pu_2(C_2O_4)_3$ occurs between 180 °C and 225 °C; however, these mechanistic proposals could not be verified by the amorphous pXRD patterns that were measured for both **Pu-160** and **Pu-200**. As described further in the discussion section, we think it's possible that dehydration destroys the long-range order of Pu(III) oxalate, which is why an amorphous pXRD pattern is seen; this also agrees with our SEM data. The detection limit of our pXRD is ~ 5%, so if there was crystalline Pu in **Pu-160**, it would have been below detection limits, though it is most likely that the material was amorphous.

pXRD measurements of **Pu-250** (Fig. 1 and Fig. S2) resulted in weakly diffracting broad peaks that were mostly consistent with the published powder diffraction file for PuO_2 (PDF #00-067-0018).[27] This broadening of the XRD patterns, compared to other PDF patterns, can be attributed to the limitations of the single-crystal X-ray diffractometer detector's resolution. While this factor contributes to the initial plutonium oxalates in Figure 1, the broadening of peaks in the remaining pXRD measurements become significantly more pronounced with higher calcination temperatures. This increased broadening can result from low bulk crystallinity, disorder, and/or the presence of an amorphous phase in the material. In several cases in the literature, broadness in the diffraction pattern of PuO_2 has been associated with nanocrystalline PuO_2.[6, 25] A few weak peaks that were inconsistent with PuO_2 were observed around 10° 2θ and between 30° and 40° 2θ, which we attribute to residual Pu(III) oxalate from incomplete calcination to PuO_2 due to the relatively low calcination temperature (i.e., 250 °C). TGA plots published by De Almeida et al. showed that conversion from $Pu_2(C_2O_4)_3$ to PuO_2 occurs around 225 - 400 °C; thus, our study confirms that 250 °C is in fact hot enough to trigger

the initial formation of PuO_2, though our vibrational spectroscopy measurements (vide infra) show that this conversion likely proceeds through an intermediate of plutonium oxalate-carbonate.

The pXRD patterns of both **Pu-300** and **Pu-450** (Fig. 1 and Fig. S2) were similar to **Pu-250**, but were entirely consistent with PuO_2 and contained no stray peaks from residual chemical phases. Additionally, the diffraction peaks of **Pu-300** and **Pu-450** were noticeably sharper than the peaks observed for **Pu-250**, which indicate that the broadening observed in **Pu-250** is most likely due to the low calcination temperature, which produces in a weakly ordered PuO_2 structure.

3.2 Scanning Electron Microscopy (SEM)

Scanning electron micrographs of each Pu-bearing sample are shown in Fig. 2. Using a lexicon of descriptive terms for characterizing particle morphology,[28] the morphology of the **Pu-25** sample is best described as *complex* particles of *mixed* morphology due to *agglomerates* and *faceted crystalline* material (Fig. 2 and Fig. S3). **Pu-25** is composed of single *bladed* crystals and *radiating columnar rosettes*. Particle faces appeared to be *euhedral* with an overall *smooth* surface, while individual isolated sub-particles appeared to have *surface inclusions*. Subtle changes in surface appearance and patterns were observed for the thermal decomposition products but the overall morphology and shape of all samples remained consistent with the baseline material (i.e., **Pu-25**). After thermal degradation at 160 °C and 200°C (**Pu-160** and **Pu-200**), additional *surface striation* patterns were observed (Fig. 2, Fig. S4, and Fig. S5), whereas the morphology of the thermal degradation products at 250 °C (Fig. 2 and Fig. S6), 300 °C (Fig. 2 and Fig. S7), and 450 °C (Fig. 2 and Fig. S8) transitions from *smooth* surfaces to *somewhat smooth* surfaces with *surface cracks* and *fractures*. The latter could be a sign of dehydration and degassing. Previous studies of oxalate decomposition have shown that CO_2 is formed as oxalate ligands decompose in air.[4-5] Interestingly, although Pu(III) oxalate converted to a disordered PuO_2 and then a more ordered PuO_2 as the material was exposed to higher temperatures, the only observed morphological change during this transition was *cracking* and *fracturing of the crystallites*. It is important to note that the Pu-25 has long range order as demonstrated by the sharp bands in the XRD spectrum. However, as the material decomposes at elevated temperatures, the transition of the oxalate to the oxide begins with the formation of amorphous nanoparticulate. Raman and XRD data of PuO_2 produced from the decomposition of Pu(IV) oxalate show phonon confinement as observed in the T_{2g} band in the Raman spectrum and corresponding broadening of the X-ray diffraction pattern – an observation consistent our prior works.[5, 17] The oxide formation from the decomposition of the Pu(III) oxalate follows the same pattern as observed with XRD (Raman features at low calcination temperatures were obfuscated by fluorescence). As the calcination temperature was increased, PuO_2 crystallites became much larger in size. It is also expected that the change in oxidation state from +3 to +4 affects the symmetry of the lattice – even though the gross morphology of the crystallites as observed by SEM remains constant.

3.3 Vibrational Spectroscopy (Raman and IR)

Raman and IR band positions for all measured samples are provided in Table 1. To the best of our knowledge, this marks the first time that Raman spectra have been reported for the thermal decomposition products of Pu(III) oxalate, although Tamain et al. previously published a single Raman spectrum of $Pu_2(C_2O_4)_3(H_2O)_6 \bullet n(H_2O)$.[23] Bands were assigned to chemical moieties based on comparison with vibrational spectra of related compounds.[23, 29-32] Compiling and assigning these

spectral bands is a major aspect of this study since this information can be used with pXRD and previously-published TGA measurements[15] to elucidate details of the structural and chemical transformations that occur during thermal decomposition of Pu(III) oxalate. Additionally, these vibrational energies can be used to evaluate the accuracy of proposed, DFT-derived chemical structures, as was done recently in studies involving Pu(IV) oxalate.[14, 24]

After curve fitting to elucidate all spectral bands, the Raman spectrum of **Pu-25** (i.e., $Pu_2(C_2O_4)_3 \bullet 9(H_2O)$) contains approximately 18 bands between 100 cm^{-1} and 3,000 cm^{-1} (Fig. 3). The most intense bands in this spectrum are double bands centered around 504, 917, and 1476 cm^{-1} corresponding to δ(OCO), ν(C-C), and ν(CO), respectively. The center of each of these three double bands are within 3 cm^{-1} of those reported in the Raman spectrum of $Pu_2(C_2O_4)_3(H_2O)_6 \bullet n(H_2O)$ by Tamain et al.[23] The spectrum acquired by Tamain et al. had a smaller spectral window (~ 400–2000 cm^{-1}) and higher noise that obscured the weaker band we observed in **Pu-25** at 858 cm^{-1}. The IR spectrum of **Pu-25** (Fig. 4) contains approximately 12 bands between 700 cm^{-1} and 5,500 cm^{-1} and an intense broad band between ~2500 cm^{-1} and 3,600 cm^{-1}. The broad band is due to an assemblage of bands from symmetric and asymmetric stretch vibrations of hydrogen bonded –OH groups from water in $Pu_2(C_2O_4)_3 \bullet 9(H_2O)$. The IR spectrum of **Pu-25** is mostly similar to the spectrum of Pu(III) oxalate recently published by Corbey et al.,[6] although very slight differences exist in the quantity and energies of the observed IR bands. We attribute these spectral differences to effects caused by radiolytic aging. Whereas Corbey et al. analyzed 5.5-month-old and 8-month-old Pu(III) oxalate, our samples of **Pu-25** were analyzed within 3 days of production. Thus, to the best of our knowledge, the IR spectrum of **Pu-25** shown in Fig. 4 is the first high-resolution IR spectrum that has been published for a freshly prepared sample of $Pu_2(C_2O_4)_3 \bullet 9(H_2O)$.

The Raman spectrum of **Pu-160** contains several bands between 100 cm^{-1} and 3,000 cm^{-1} (Fig. 3). The spectrum of **Pu-160** is markedly different than the Raman spectrum of **Pu-25**; this is most evident when looking at the broad spectral features between 1,760 cm^{-1} and 2,870 cm^{-1}, which correspond to fluorescence. In **Pu-160**, several features were observed that were not present in the spectrum of **Pu-25**. Furthermore, bands that were clearly discernible in the **Pu-25** spectrum between 2,900 cm^{-1} and 3000 cm^{-1} were not readily discernible in the **Pu-160** spectrum. Multiple bands between 90 cm^{-1} and 300 cm^{-1} that were observed in **Pu-25** were replaced by a single broad band in this area in the **Pu-160** spectrum. Additionally, two bands located at 1,625 cm^{-1} and 1,725 cm^{-1} grew in intensity with increasing temperature from **Pu-25** to **Pu-160** (and **Pu-200)**, indicating they are associated with decomposition in the material. When combined with the noticeable differences between the pXRD patterns of **Pu-25** and **Pu-160**, these Raman results make it clear that the structure of Pu(III) oxalate begins to decompose when the material is heated from room temperature up to 160 °C. Interestingly the features observed at 1,625 cm^{-1} and 1,725 cm^{-1} in **Pu-160** are similar in location to a broad band observed at 1,608 cm^{-1} during the thermal decomposition of Pu(IV) oxalate, so perhaps there is some similarity between the structures.[5]

Marked differences between **Pu-25** and **Pu-160** were also evident from IR measurements (Fig. 4). The IR spectrum of **Pu-160** contains approximately 11 bands between 800 cm^{-1} and 5,500 cm^{-1} compared to the 12 bands observed for **Pu-25**. **Pu-160** also shows growth in the spectrum background between 1,200 cm^{-1} and 1,800 cm^{-1} relative to **Pu-25**. The **Pu-160** spectrum contains an intense broad band between ~2,500 cm^{-1} and 3,600 cm^{-1}, which is similar to **Pu-25** and corresponds to the –OH stretch absorption band; however, **Pu-160** contains an intense band between 2,100 cm^{-1} and 2,300 cm^{-1} that was completely absent from the **Pu-25** spectrum. This band has been identified as adsorbed CO_2 in the material, and was also observed during the thermal decomposition of Pu(IV) oxalate.[5]

The Raman spectrum of **Pu-200** was mostly similar to the spectrum of **Pu-160**, although the broad bands observed between 1,760 cm^{-1} and 2,870 cm^{-1} in **Pu-160** were reduced in width and intensity in the spectrum of **Pu-200,** and a new, weak band at 1,310 cm^{-1} was observed. The IR spectrum of **Pu-200** (Fig. 4) contains 16 bands between 800 cm^{-1} and 5,500 cm^{-1}. The spectrum also contains the intense broad band between ~2,500 cm^{-1} and 3,600 cm^{-1} that was seen in the IR spectrum of **Pu-25** and **Pu-160**. Like **Pu-160**, the IR spectrum of **Pu-200** contains several intense bands between 2,100 cm^{-1} and 2,300 cm^{-1}.

Although the Raman spectra of **Pu-25**, **Pu-160**, and **Pu-200** were measured with high signal-to-noise, spectra measured for **Pu-250** and **Pu-300** were saturated with a broad fluorescence signal that precluded assignment of Raman modes (Fig. S9). Spectra acquired at different spots within these samples repeatedly exhibited this strong fluorescence feature, obfuscating any detectable spectroscopic information. Conversely, IR spectra of **Pu-250** and **Pu-300** were measured with a high signal-to-noise ratio (Fig. 4). For **Pu-250**, 13 bands were observed between 800 cm^{-1} and 5,500 cm^{-1}. For **Pu-300**, 9 bands were observed between 800 cm^{-1} and 5,500 cm^{-1}. For both materials, the broad water band between ~ 2,500 cm^{-1} and 3,600 cm^{-1} was present, although the intensity of this band was slightly lower compared to the same band in **Pu-25**, **Pu-160**, and **Pu-200.** Reduction in the intensity of this band indicates that the increased temperature facilitated the removal of water from these samples. This result is consistent with TGA data published by De Almeida et al., which showed that dehydration of Pu(III) oxalate occurs up to 225 °C.[15] The peak observed at 1,717 cm^{-1} in **Pu-25** shifted to 1,727 cm^{-1} and 1,725 cm^{-1} for **Pu-160** and **Pu-200**, respectively. This peak, which is assigned to the C=O bond of the oxalate group, indicates a rearrangement of the ligands between the Pu atoms and the oxalate groups due to dehydration. A progressive decrease in the number of bands was observed between 1,500 cm^{-1} and 1,900 cm^{-1} for **Pu-200 → Pu-250 → Pu-300.** Comparison of this result with pXRD measurements suggests that the 1,200 – 1,800 cm^{-1} spectral region is very sensitive to the structural changes incurred as Pu(III) oxalate breaks down. Thus, this spectral region showed the largest difference between samples produced at lower temperatures (**Pu-25**, **Pu-160**, **Pu-200**) and samples produced at higher temperatures (**Pu-250** and **Pu-300**).

Unlike the Raman spectra of **Pu-250** and **Pu-300**, which were saturated by fluorescence, the spectrum of **Pu-450** had a high signal-to-noise with no fluorescence. The Raman spectrum of **Pu-450** contained 9 bands with the most intense bands at 479; 2,135; and 2,638 cm^{-1}, which correspond to the T_{2g}, $\Gamma_1 \rightarrow \Gamma_5$ electronic transition, and $\Gamma_1 \rightarrow \Gamma_3$ electronic transitions of PuO_2, respectively. This spectrum is entirely consistent with previously published spectra of PuO_2.[19-22] The most variable band in the PuO_2 Raman spectrum corresponds to the defect band, located at 580 cm^{-1} which appears in the spectrum with age and is related to alpha radiolytic damage in the material. This band most likely corresponds to the IR LO1 band which becomes active in the Raman spectrum in the amorphous material (due to a crystal symmetry change). Our previous research has shown that there are four Raman bands in the defect band region and most likely their presence is related to unknown sub-oxide species created by the alpha decay in the material. These defects can be annealed at high calcination temperatures resulting in the elimination of the defect bands from the Raman spectrum. Similar defect bands have been observed in UO_2 and CeO_2.[33-37] In the UO_2 system, U_4O_9 has been postulated to be produced during irradiation.[38] Meanwhile, in CeO_2, Ce^{3+} oxidation state has been used to explain some of the bands in this region. Future computational modeling will be needed to provide understanding on the emergence of defect bands with alpha decay.

Lastly, the IR spectrum of **Pu-450** contained 11 bands and was dramatically different than the spectra of all lower-temperature samples; a result consistent with pXRD results which is consistent with the assignment of **Pu-450** as pure-phase, more crystalline PuO_2.

4. Discussion

Comprehensive understanding of the chemical transitions and structural perturbations incurred by solid-state nuclear fuel cycle compounds has wide-reaching applications in radiochemical fields, such as nuclear nonproliferation, nuclear forensics, and nuclear fuel and waste reprocessing. Although the Pu oxalate method has been used to produce PuO_2 for over 80 years, the exact details of the chemical and structural transformations that occur as Pu(III) oxalate dehydrates and eventually oxidizes to PuO_2 has remained scarce in the literature.

By combining pXRD, SEM, and IR and Raman spectroscopy measurements, an exceptionally clear view of the thermal decomposition of Pu(III) oxalate was gained. Each technique filters a given property of the observed material. pXRD observes long range crystallinity and is not able to quantify the amorphous species in the material. In contrast, vibrational spectroscopy provides information on the molecular bonds and chemical structures. Raman spectroscopy depends on the polarizability of the electrons in the bonds while infrared spectroscopy depends on the change of the dipole moment. Selection rules can affect the intensity of the bands in the spectra. Since each technique has strengths and weaknesses to the detection of species in a material, it is not uncommon that one technique indicates the existence of a molecular moiety and while the others do not. Indeed, this is the case in the thermal decomposition of plutonium oxalates. While pXRD can observe the formation of PuO_2 nanoparticulate, the technique is blind to any amorphous Pu oxalate-carbonate species. In contrast, infrared spectroscopy can show the presence of the oxalate-carbonate species but cannot show any interaction with Pu in PuO_2 since frequencies related to Pu-oxygen are in the far-infrared spectral region (360 – 500 cm^{-1} depending on the size of the crystals and ~290 cm^{-1}).[39] Far IR bands are not observable in our present experimental setup (double-walled cells) which utilize BaF_2 windows and limit transmission in the infrared to 800 cm^{-1}. Although Raman spectroscopy can observe the oxygen movement around the plutonium atom in the T_{2g} band and the oxalate and carbonate species, fluorescence from minor impurities can greatly affect the observables.

The first observation from our measurements is that Pu(III) oxalate precipitated from nitric acid at room temperature (**Pu-25**) is in the form of $Pu_2(C_2O_4)_3 \bullet 9(H_2O)$. The gross morphology of this product features *bladed* crystals and *radiating columnar rosettes.* The Raman and IR spectra of this compound feature vibrational modes consistent with Pu–O and oxalate structural moieties. The precise resonance energies extracted from both IR and Raman measurements can be used in future studies to verify the authenticity of computationally derived molecular and lattice structures for $Pu_2(C_2O_4)_3 \bullet 9(H_2O)$. These energies can also be used to identify nuclear materials of unknown origin for nuclear forensics and nonproliferation purposes.

While **Pu-25** can be neatly defined as $Pu_2(C_2O_4)_3 \bullet 9(H_2O)$, the chemical formulae for **Pu-160** and **Pu-200** are less clear. Notably, both **Pu-160** and **Pu-200** have gross morphologies similar to **Pu-25**, although **Pu-200** has more *surface striation*. One observation that is clear, is that both **Pu-160** and **Pu-200** contain less water than **Pu-25**, as indicated by a reduction in the intensity of water bands in the IR spectra and the formation of CO_2 from the decomposition of the oxalate. Although Pu(III) oxalate dehydration can be clearly observed in our study, we must point out that the possibility of our samples acquiring water from the environment during sample handling is always possible; thus, quantitative assessments of water content cannot be performed.

Pu-160 and **Pu-200** also produce vibrational spectra consistent with oxalate structural moieties, similar to **Pu-25**, but show carbonate formation, similar to what was observed in the thermal decomposition of $Pu^{IV}(C_2O_4)_2$.[5, 29] The baseline of the IR spectra for **Pu-160** and **Pu-200** are elevated relative to **Pu-25** in the 1,200 cm^{-1} to 1,800 cm^{-1} spectral region. This is an important spectral region

as it contains two bands that are consistent with oxalate-carbonate moieties, which we postulate are of the type $Pu^{III}(C_2O_4)_x(CO_3)_y$. This result is similar to what has been observed during the thermal decomposition of $Pu^{IV}(C_2O_4)_2$.[5, 29] Another noteworthy difference in the IR spectrum of **Pu-160 and Pu-200** compared to **Pu-25**, is the emergence of a sharp band at ~2,340 cm^{-1}, which corresponds to adsorbed CO_2 that is released during oxalate degradation.[29] CO_2 is a linear molecule with three different fundamental vibrations. In the infrared, CO_2 has two vibrational modes corresponding to the bending mode (667 cm^{-1}) and an asymmetric stretch (2349 cm^{-1}). Free CO_2 also has IR-active rotational bands; however, this is not observed for CO_2 adsorbed on surfaces.[40] The asymmetric stretch for adsorbed CO_2 has been observed over a wide range – from 2285 to 2410 cm^{-1}. The CO_2 spectral region for the **Pu-160**, **Pu-200** and **Pu-250** spectra show markedly different CO_2 frequencies indicating different adsorption sites/strengths. For the **Pu-160**, the bands which most likely corresponding to CO_2 were observed at 2386, 2341 (dominant), and at 2277 cm^{-1}. Meanwhile, for **Pu-200**, bands were observed for 2386, 2343 (most dominant and broad), 2277, and 2229 cm^{-1} suggesting multiple different chemical environments for adsorbed CO_2. Thereafter, **Pu-250** shows 2345, 2276, and 2228 cm^{-1} showing similar chemical environments. Once the Pu oxalates have been more thermally degraded (e.g., **Pu-300)**, only two CO_2 bands are observed at 2340 and 2273 cm^{-1}. The numerous species observed for each decomposition temperature suggests that different chemical environments exist for surface-adsorbed CO_2 in the Pu oxalate carbonate, Pu carbonate, and Pu oxide chemical moieties. Given the obvious reduction in lattice water, the observation of oxalate-carbonate signatures in the 1,200 cm^{-1} to 1,800 cm^{-1} spectral region, and the clear observation of CO_2 in these materials, it is reasonable to assume that Pu(III) oxalate calcined at 160 °C and 200 °C have chemical formulae similar to a mixture of $Pu_2(C_2O_4)_3 \cdot x(H_2O)$ and $Pu^{III}(C_2O_4)_x(CO_3)_y$ with CO_2 dispersed and adsorbed to the surface of different moieties in the lattice. These chemical assignments contrast with the observations of De Almeida et al., whose TGA measurements showed that **Pu-160** is likely $Pu_2(C_2O_4)_3 \cdot 2(H_2O)$ or $Pu_2(C_2O_4)_3 \cdot (H_2O)$ while **Pu-200** is likely $Pu_2(C_2O_4)_3 \cdot (H_2O)$ or $Pu_2(C_2O_4)_3$.[15] Oxalate-carbonate species were never identified in previous TGA-based studies, though they are clearly observed in our IR data. The observation of oxalate-carbonate moieties during the thermal decomposition of Pu(III) oxalate is consistent with observations made during the thermal decomposition of Pu(IV) oxalate, thus indicating the decomposition mechanisms are similar despite the different oxidation state of Pu at the start of decomposition.

The amorphous pXRD patterns of both **Pu-160** and **Pu-200** preclude assignment of exact chemical structures for these materials; however, using the detailed spectroscopic energies in Table 1 as a guide, future computational efforts should be able to elucidate potential structures that form at the Pu(III) oxalate lattice is thermal decomposed. One explanation why the pXRD patterns of **Pu-160** and **Pu-200** are broad is that calcination not only removes water from the Pu(III) oxalate lattice, but in doing so, it reduces long-range crystallinity of the material, thus leading to measurements of an amorphous pXRD pattern. *While TGA data by De Almeida et al. showed direct conversion of Pu(III) oxalate to PuO_2, our data clearly show the presence of carbonate species during thermal decomposition of Pu(III) oxalate, which is a previously unreported result.[15] These results highlight the utility of using multiple analytical methods to elucidate the oxalate degradation mechanism.*

Both TGA and vibrational spectroscopy studies of the thermal decomposition of Pu(IV) oxalate have shown the formation of multiple carbonate-containing structures: $Pu(C_2O_4)(CO_3)_{1/2}$, $Pu(C_2O_4)_{1/2}(CO_3)$, and $PuOCO_3$. In this case, the oxidation state of plutonium during thermal decomposition changes from +IV to +III and back to +IV as Pu(IV) oxalate converts to carbonate and oxycarbonate species just before PuO_2 forms. In the case of Pu(III) oxalate, our spectroscopy measurements of **Pu-160** and **Pu-200** show that the carbonate band is present in the spectra of both

materials, which is incongruent with the TGA results of De Almeida. Given the clear presence of oxalate and carbonate bands during the thermal decomposition of Pu(III) oxalate, it may be possible that plutonium changes its oxidation state from 3+ to 4+ prior to the formation of PuO_2. Since Pu(III) and Pu(IV) will have different bond lengths, a change in the plutonium oxidation state could impact long-range ordering without affecting bulk material morphology - as was observed in our SEM measurements.

For **Pu-250**, **Pu-300**, and **Pu-450**, pXRD measurements clearly establish the presence of PuO_2, though IR spectroscopy shows that **Pu-250** and **Pu-300** still contain CO_2 adsorbed to surface sites and molecular bands corresponding oxalate-carbonate species. Our pXRD data also suggest that **Pu-250** contains a secondary chemical phase or chemical residue, as indicated by a few diffraction peaks that are inconsistent with PuO_2. Based on IR measurements, we suspect this chemical phase is a mixture of $Pu(C_2O_4)(CO_3)_{1/2}$, $Pu(C_2O_4)_{1/2}(CO_3)$, and possibly $PuOCO_3$ with adsorbed CO_2 and some carbonaceous residue due to incomplete removal of the oxalate ligand during low-temperature calcination.[4] The gross morphology of the thermal degradation products at 250 °C, 300 °C, and 450 °C transitions from *smooth* surfaces to *somewhat smooth* surfaces with *surface cracks* and *fractures* at higher calcination temperatures. This cracking could be caused by degassing of water as the oxalate structures completely dehydrate and/or by CO_2, which is a degradation product of the oxalate ligand.

The crystallinity of PuO_2 formed from Pu(III) oxalate is dependent on the temperature of calcination. PuO_2 formed at 250 °C exhibits broad diffraction peaks that appear consistent with a disordered lattice structure for PuO_2.[6, 25] Conversely, pXRD measurement of **Pu-300** yield diffraction patterns with narrower peaks, with IR indicating $Pu(CO_3)_2$, and narrower still for **Pu-450**, with Raman showing the T_{2g} band indicative of PuO_2 indicating that transformation from disordered PuO_2 to a more ordered PuO_2 occurring as the calcination temperature is increased. Nanocrystalline PuO_2 has also been associated with PuO_2 that forms from auto-decomposition of Pu(III) oxalate due to self-radiolysis.[6] The importance of these observations regarding the crystallinity of PuO_2 cannot be understated. *It is clear from our work herein and the work of Corbey et al. that the size of the PuO_2 crystallites can be used as a physicochemical indicator of the materials production/storage history.*[6] This type of information is crucial for determining material provenance for nuclear forensics and nonproliferation purposes.

Although pXRD patterns of **Pu-250**, **Pu-300** shows the formation of PuO_2, IR indicates that most of the material calcined in **Pu-250** is in the form $Pu(C_2O_4)(CO_3)_{1/2}$, $Pu(C_2O_4)_{1/2}(CO_3)$, and $Pu(CO_3)_2$ at **Pu-300.** At **Pu-450**, Raman and pXRD are consistent with PuO_2, while IR shows the elimination of the CO_3 band. Specifically, both **Pu-250** and **Pu-300** exhibited intense fluorescence in every Raman measurement (Fig. S9). Strong fluorescence was observed in the Raman spectrum of these samples at every tested laser wavelength. Interrogating the material with either 405, 514, 633, or 785 nm lasers yielded the same broad fluorescence feature in the resultant spectrum. This contrasted with **Pu-200** and **Pu-450**, which both produced Raman spectra with excellent signal-to-noise and no obvious fluorescence. Considering that De Almeida et al. used TGA to show that conversion from Pu(III) oxalate to PuO_2 occurs between 225 °C and 400 °C and considering that both **Pu-250** and **Pu-300** have been confirmed as containing PuO_2 based on their pXRD patterns, we postulate that the origin of fluorescence in **Pu-250** and **Pu-300** is the presence of carbonaceous species that form as the oxalate ligand decomposes. Previously published computational assessment of the thermal decomposition of oxalic acid has shown possible decomposition products of CO_2, CO, H_2O, and other polyaromatic compounds, which are highly fluorescent at the wavelengths used in this study.[5, 41] When looking at the IR spectra of **Pu-250** and **Pu-300** for further clues about residual carbon, we find that **Pu-250** has bands at 1,376 cm^{-1} and 1,544 cm^{-1} and **Pu-300** has bands at 1,378

cm^{-1} and 1,547 cm^{-1}. These bands are consistent with carbonates and are not seen in **Pu-200** or **Pu-450**. The shape of the bands observed in **Pu-300** correspond to $PuOCO_3$, similar to what was observed in the thermal decomposition of Pu(IV) oxalate at 350 °C.[5]

This result is quite interesting as it shows that important decomposition mechanics occur at the onset of PuO_2 formation, such that decomposition products from the oxalate ligand provide spectroscopic clues that can be used to estimate a materials calcination temperature.[41]

Unlike PuO_2 produced at 250 °C and 300 °C, the Raman spectrum of PuO_2 produced at 450 °C (**Pu-450**) showed no fluorescence and was quite consistent with the literature spectrum for PuO_2.[16, 19-22] The same can be said about the IR spectrum for **Pu-450**; however, both IR and pXRD data still suggest the presence of a small amount of residual amorphous carbonaceous material.

5. Conclusions

The thermal decomposition of Pu(III) oxalate was studied in detail using a battery of physicochemical techniques, including pXRD, SEM, and IR and Raman spectroscopy. Together, these results clearly show the chemical transitions and structural perturbations incurred by Pu(III) oxalate as it is heated in air to form dehydrated oxalate and carbonate molecular species with subsequent conversion to $PuOCO_3$ and then PuO_2. As the temperature is elevated, the material undergoes a progressive dehydration until the oxalate ligands begin to decompose to CO_2 and carbonate species. Once the temperature reaches 450 °C, pXRD and Raman spectroscopy reveal nearly full conversion to PuO_2. At temperatures between 200 °C and 350 °C, a strong fluorophore is formed in the material, obfuscating Raman spectroscopic observation until the material is fully calcined to PuO_2. At these intermediate temperatures, IR spectroscopy details a rich progression of bands in the 1200–1800 cm^{-1} region, which have potential to "fingerprint" a quantity of Pu(III) oxalate heated to a given temperature en route to PuO_2. Although a previous TGA-based mechanistic study of Pu(III) oxalate thermal degradation reports direct conversion from the oxalate to PuO_2, our results reveal the presence of carbonate molecules, which may correspond to Pu oxalate carbonate or Pu carbonate, as is observed when Pu(IV) oxalate is thermally decomposed to PuO_2. In summary, the data provided herein demonstrate the rich spectroscopic nature of a rather underexplored, and technologically relevant, plutonium system. Ideally these results, and the ancillary XRD and SEM data will further future investigations into the Pu(III) oxalate system both experimentally and computationally.

Declaration of Competing Interest

The authors declare that they have no known competing financial interests or personal relationships that could have appeared to influence the work reported in this paper.

CRediT authorship contribution statement

Jonathan H. Christian: Funding acquisition, Conceptualization, Data curation, Writing – review & editing. **Bryan J. Foley:** Conceptualization, Data curation, Writing – review & editing. **Elodia Ciprian:** Data curation, Writing – review & editing. **Jason Darvin:** Data curation, Writing – review & editing. **Don D. Dick:** Data curation, Writing – review & editing. **Amy E. Hixon:** Funding acquisition, Conceptualization, Data curation, Writing – review & editing. **Eliel Villa-Aleman:** Funding acquisition, Conceptualization, Data curation, Writing – review & editing.

Abbreviations
DFT – density functional theory
DRIFTS – Diffuse Reflectance Infrared Fourier Transform Spectroscopy
FWHM – full width at half maximum
IR – infrared
pXRD – powder X-ray diffraction
SEM – scanning electron microscopy
S/N – signal to noise
TGA – thermogravimetric analysis

Acknowledgements
This work was produced by Battelle Savannah River Alliance, LLC under Contract No. 89303321CEM000080 and/or a predecessor contract with the U.S. Department of Energy. Publisher acknowledges the U.S. Government license to provide public access under the DOE Public Access Plan (http://energy.gov/downloads/doe-public-access-plan). We would like to thank our sponsor, the DOE National Nuclear Security Administration Office of Defense Nuclear Nonproliferation Research and Development, and our program manager Allen J. Bakel for support. We also wish to acknowledge the SRNL Laboratory Directed Research & Development under the project LDRD-2016-00015 for procurement of some equipment and investment in project development. We also would like to acknowledge Mr. Michael Maxwell and Mr. Ross Smith for engineering and assembly of double-walled cells used for this work.

References

1. Wick, O. J., *Plutonium Handbook: A Guide to the Technology*; American Nucear Society: La Grange Park, IL, 1980.
2. Patterson, J. P.; Parkes, P., *Recycling Uranium and Plutonium*; Oxford University Press: United Kingdom, 1996.
3. Hammons, J. A.; Nielsen, M. H.; Bagge-Hansen, M.; Lauderbach, L. M.; Hodgin, R. L.; Bastea, S.; Fried, L. E.; Cowan, M. R.; Orlikowski, D. A.; Willey, T. M., Observation of Variations in Condensed Carbon Morphology Dependent on Composition B Detonation Conditions. *Propellants, Explosives, Pyrotechnics* **2020**, *45*, 347-355.
4. Orr, R. M.; Sims, H. E.; Taylor, R. J., A Review of Plutonium Oxalate Decomposition Reactions and Effects of Decomposition Temperature on the Surface Area of the Plutonium Dioxide Product. *Journal of Nuclear Materials* **2015**, *465*, 756-773.
5. Christian, J. H.; Foley, B. J.; Ciprian, E.; Dick, D. D.; Said, M.; Darvin, J.; Hixon, A. E.; Villa-Aleman, E., Raman and Infrared Spectra of Plutonium (Iv) Oxalate and Its Thermal Degradation Products. *Journal of Nuclear Materials* **2022**, *562*, 153574.
6. Corbey, J. F.; Sweet, L. E.; Sinkov, S. I.; Reilly, D. D.; Parker, C. M.; Lonergan, J. M.; Johnson, T. J., Quantitative Microstructural Characterization of Plutonium Oxalate Auto-Degradation and Evidence for Puo2 Nanocrystal Formation. *European Journal of Inorganic Chemistry* **2021**, *2021*, 3277-3291.
7. Myser, M. N., Thermal Decomposition of Plutonium(Iv) Oxalate and Hydrofluorination of Plutonium(Iv) Oxalate and Oxide. *United States: N. p., 1956. Web. doi:10.2172/4181389.*
8. Kartushova, R. E.; Rudenko, T. I.; Fomin, V. V., Thermal Decomposition of Tetravalent and Trivalent Plutonium Oxalates. *The Soviet Journal of Atomic Energy* **1958**, *5*, 831-835.

9. Rao, G. S.; Subramanian, M. S.; Welch, G. A., Thermal Decomposition of Plutonium Oxalates. *Journal of Inorganic and Nuclear Chemistry* **1963**, *25*, 1293-1295.
10. Glasner, A., Remarks on the Thermal Decomposition of Plutonium (Iv) Oxalates. *Journal of Inorganic and Nuclear Chemistry* **1964**, *26*, 1475-1476.
11. Jenkins, I. L.; Waterman, M. J., The Thermal Decomposition of Hydrated Plutonium(Iv) Oxalates. *Journal of Inorganic and Nuclear Chemistry* **1964**, *26*, 131-137.
12. Nissen, D. A., The Thermal Decomposition of Plutonium (Iv) Oxalate Hexahydrate. *Journal of thermal analysis* **1980**, *18*, 99-109.
13. Karelin, A. I.; Krot, N. N.; Kozlova, R. D.; Lobas, O. P.; Matukha, V. A., Thermal Decomposition of Np(Iv) and Pu(Iii, Iv) Oxalates. *Journal of Radioanalytical and Nuclear Chemistry Articles* **1990**, *143*, 241-252.
14. South, C. J.; Roy, L. E., Insights into the Thermal Decomposition of Plutonium(Iv) Oxalate – a Dft Study of the Intermediate Structures. *Journal of Nuclear Materials* **2021**, *549*, 152864.
15. De Almeida, L.; Grandjean, S.; Vigier, N.; Patisson, F., Insights into the Thermal Decomposition of Lanthanide(Iii) and Actinide(Iii) Oxalates – from Neodymium and Cerium to Plutonium. *European Journal of Inorganic Chemistry* **2012**, *2012*, 4986-4999.
16. Villa-Aleman, E.; Dick, D. D.; Christian, J. H.; Foley, B. J.; Roy, L. E., The Electronic Raman Scattering Spectrum of Puo2. *Journal of Raman Spectroscopy*, *n/a*.
17. Villa-Aleman, E.; Christian, J. H.; Darvin, J. R.; Foley, B. J.; Dick, D. D.; Fallin, B.; Fessler, K. A. S., Diffuse Reflectance Spectroscopy and Principal Component Analysis to Retrospectively Determine Production History of Plutonium Dioxide. *Applied Spectroscopy* **2023**, *77*, 449-456.
18. Villa-Aleman, E.; Dick, D. D.; Christian, J. H.; Foley, B. J., Laser-Induced Annealing of Aged Puo2. *Journal of Raman Spectroscopy*, *n/a*.
19. Villa-Aleman, E.; Bridges, N. J.; Shehee, T. C.; Houk, A. L., Raman Microspectroscopy of Puo2 Particulate Aggregates. *Journal of Nuclear Materials* **2019**, *515*, 140-149.
20. Villa-Aleman, E.; Houk, A. L.; Bridges, N. J.; Shehee, T. C., Raman Spectroscopy: A Tool to Investigate Alpha Decay Damage in a Puo2 Crystal Lattice and Determining Sample Age since Calcination. *Journal of Raman Spectroscopy* **2019**, *50*, 899-901.
21. Villa-Aleman, E.; Houk, A. L.; Shehee, T. C.; Bridges, N. J., Raman Signatures from Age-Dating Puo2 since Last Calcination. *Journal of Nuclear Materials* **2021**, *551*, 152969.
22. Sarsfield, M. J.; Taylor, R. J.; Puxley, C.; Steele, H. M., Raman Spectroscopy of Plutonium Dioxide and Related Materials. *Journal of Nuclear Materials* **2012**, *427*, 333-342.
23. Tamain, C.; Arab-Chapelet, B.; Rivenet, M.; Legoff, X. F.; Loubert, G.; Grandjean, S.; Abraham, F., Coordination Modes of Americium in the Am2(C2o4)3(H2o)6·4h2o Oxalate: Synthesis, Crystal Structure, Spectroscopic Characterizations and Comparison in the M2(C2o4)3(H2o)6·Nh2o (M = Ln, an) Series. *Inorganic Chemistry* **2016**, *55*, 51-61.
24. Isbill, S. B.; Ciprian, E.; Christian, J. H.; Hixon, A.; Foley, B. J.; Villa-Aleman, E.; Miskowiec, A. J., Computational Insights into the Lattice Dynamics of Pu(Iv) Oxalates. *Journal of Nuclear Materials* **2023**, *573*, 154106.
25. Said, M.; Hixon, A. E., Microscopy and Spectroscopy of Plutonium Dioxide Aging under Ambient and near-Ambient Conditions. *Journal of Alloys and Compounds* **2021**, *854*, 156277.
26. Sze, S. K.; Siddique, N.; Sloan, J. J.; Escribano, R., Raman Spectroscopic Characterization of Carbonaceous Aerosols. *Atmospheric Environment* **2001**, *35*, 561-568.

27. Mapelli, C.; Castiglioni, C.; Meroni, E.; Zerbi, G., Graphite and Graphitic Compounds: Vibrational Spectra from Oligomers to Real Materials. *Journal of Molecular Structure* **1999**, *480-481*, 615-620.
28. Tamasi, A. L., et al., A Lexicon for Consistent Description of Material Images for Nuclear Forensics. *Journal of Radioanalytical and Nuclear Chemistry* **2016**, *307*, 1611-1619.
29. Vigier, N.; Grandjean, S.; Arab-Chapelet, B.; Abraham, F., Reaction Mechanisms of the Thermal Conversion of Pu(Iv) Oxalate into Plutonium Oxide. *Journal of Alloys and Compounds* **2007**, *444-445*, 594-597.
30. K. Nakamoto, *Infrared and Raman Spectra of Inorganic and Coordination Compounds - Application in Coordination, Organometallic, and Bioinorganic Chemistry*: Wiley, Hoboken, NJ, 2009.
31. Desfougeres, L.; Welcomme, É.; Ollivier, M.; Martin, P. M.; Hennuyer, J.; Hunault, M. O. J. Y.; Podor, R.; Clavier, N.; Favergeon, L., Oxidation as an Early Stage in the Multistep Thermal Decomposition of Uranium(Iv) Oxalate into U3o8. *Inorganic Chemistry* **2020**, *59*, 8589-8602.
32. Frost, R. L.; Weier, M. L., Raman Spectroscopy of Natural Oxalates at 298 and 77 K. *Journal of Raman Spectroscopy* **2003**, *34*, 776-785.
33. Elorrieta, J. M.; Bonales, L. J.; Baonza, V. G.; Cobos, J., Temperature Dependence of the Raman Spectrum of Uo2. *Journal of Nuclear Materials* **2018**, *503*, 191-194.
34. Elorrieta, J. M.; Bonales, L. J.; Rodríguez-Villagra, N.; Baonza, V. G.; Cobos, J., A Detailed Raman and X-Ray Study of Uo2+X Oxides and Related Structure Transitions. *Physical Chemistry Chemical Physics* **2016**, *18*, 28209-28216.
35. Filtschew, A.; Hofmann, K.; Hess, C., Ceria and Its Defect Structure: New Insights from a Combined Spectroscopic Approach. *The Journal of Physical Chemistry C* **2016**, *120*, 6694-6703.
36. Taniguchi, T.; Watanabe, T.; Sugiyama, N.; Subramani, A. K.; Wagata, H.; Matsushita, N.; Yoshimura, M., Identifying Defects in Ceria-Based Nanocrystals by Uv Resonance Raman Spectroscopy. *The Journal of Physical Chemistry C* **2009**, *113*, 19789-19793.
37. Xu, Y.; Wang, F.; Liu, X.; Liu, Y.; Luo, M.; Teng, B.; Fan, M.; Liu, X., Resolving a Decade-Long Question of Oxygen Defects in Raman Spectra of Ceria-Based Catalysts at Atomic Level. *The Journal of Physical Chemistry C* **2019**, *123*, 18889-18894.
38. Desgranges, L.; Baldinozzi, G.; Simon, P.; Guimbretière, G.; Canizares, A., Raman Spectrum of U4o9: A New Interpretation of Damage Lines in Uo2. *Journal of Raman Spectroscopy* **2012**, *43*, 455-458.
39. Hudry, D., et al., Ultra-Small Plutonium Oxide Nanocrystals: An Innovative Material in Plutonium Science. *Chemistry – A European Journal* **2014**, *20*, 10431-10438.
40. Busca, G.; Lorenzelli, V., Infrared Spectroscopic Identification of Species Arising from Reactive Adsorption of Carbon Oxides on Metal Oxide Surfaces. *Materials Chemistry* **1982**, *7*, 89-126.
41. Higgins, J.; Zhou, X.; Liu, R.; Huang, T. T. S., Theoretical Study of Thermal Decomposition Mechanism of Oxalic Acid. *The Journal of Physical Chemistry A* **1997**, *101*, 2702-2708.
42. Nakamoto, K., *Infrared and Raman Spectra of Inorganic and Coordination Compounds - Application in Coordination, Organometallic, and Bioinorganic Chemistry*; Wiley: Hoboken, NJ, 2009.
43. Schmidt, P.; Badou, A.; Fröhlich, F., Detailed Ft near-Infrared Study of the Behaviour of Water and Hydroxyl in Sedimentary Length-Fast Chalcedony, Sio2, Upon Heat Treatment. *Spectrochimica Acta Part A: Molecular and Biomolecular Spectroscopy* **2011**, *81*, 552-559.

44. McIntosh, I. M.; Nichols, A. R. L.; Tani, K.; Llewellin, E. W., Accounting for the Species-Dependence of the 3500 Cm−1 H2ot Infrared Molar Absorptivity Coefficient: Implications for Hydrated Volcanic Glasses. *American Mineralogist* **2017**, *102*, 1677-1689.

TABLE 1

Band positions for the vibrational spectra of Pu(III) oxalate produced at room temperature (**Pu-25**) and its degradation products when heated up to 450ºC (**Pu-450**); band positions in cm^{-1}. Bands of similar wavenumbers are compiled in the same row. When practical, band assignments are listed and are based on comparison with related compounds; bands that could not be unambiguously assigned are not labeled.[29, 31, 42-44]

Pu-25		**Pu-160**		**Pu-200**		**Pu-250**		**Pu-300**		**Pu-450**		**Approximate vibrational mode assignments**
IR	*Raman*	*IR*	*Raman*	*IR*	*Raman*	*IR*	*Raman*	*IR*	*Raman*	*IR*	*Raman*	
	110											Pu-O and lattice
	177											Pu-O and lattice
	239		210		210							Pu-O and lattice
											479	T_{2g} of PuO_2
	498, 511		498, 512		498, 512							δ(OCO)
											585	Defect band of PuO_2
				812			Spectrum was saturated by fluorescence		Spectrum was saturated by fluorescence			ν(OCO) and Pu-O
	858		854	842	853	839		824				$\nu(CO_3)$
	911,		907,	913	909,	909		900		882		ν(C-C)
899	922	914	918		920							
1037		1049	1064	1077	1064	1076		1065		1042		ν(C-C)
										1101		ν(C-O)
				1163								
											1166	2LO2 of PuO_2
1263								1263		1262		
1319		1321		1323	1310							ν(CO) + d(OCO)
						1376		1378				ν(CO) + ν(C-C)
1355												
	1413		1397		1395							ν(CO)
										1412		OH bending
	1471,		1467,		1467,							
1477	1481	1468	1481	1474	1483							ν(CO)
						1544		1547		1536		
												$\nu(RCO_2)$ + ν(RCO)
1586		1577		1602								
	1621		1622		1625					1637		ν(C-O)

1717	1718	1727	1710	1725	1704	1696					ν(CO-H)
		1897		1898							
										2135	$\Gamma_1 \rightarrow \Gamma_5$ electronic transition of PuO_2
				2138							
2198				2229							
2276		2278		2277		2277					
2347		2340		2344		2345		2339			ν(CO_2)
		2387		2386							
			2500		2450	2582					
										2638	$\Gamma_1 \rightarrow \Gamma_3$ electronic transition of PuO_2
	2700		2700						2726		
	2872								2874	2868	C-H stretch
	2905									2906	C-H stretch
	2942					2933		2933	2933	2933	C-H stretch
	2964		2950		2950	2965		2965	2962	2964	C-H stretch
						3700					
5198		5157		5146		5150					H_2O

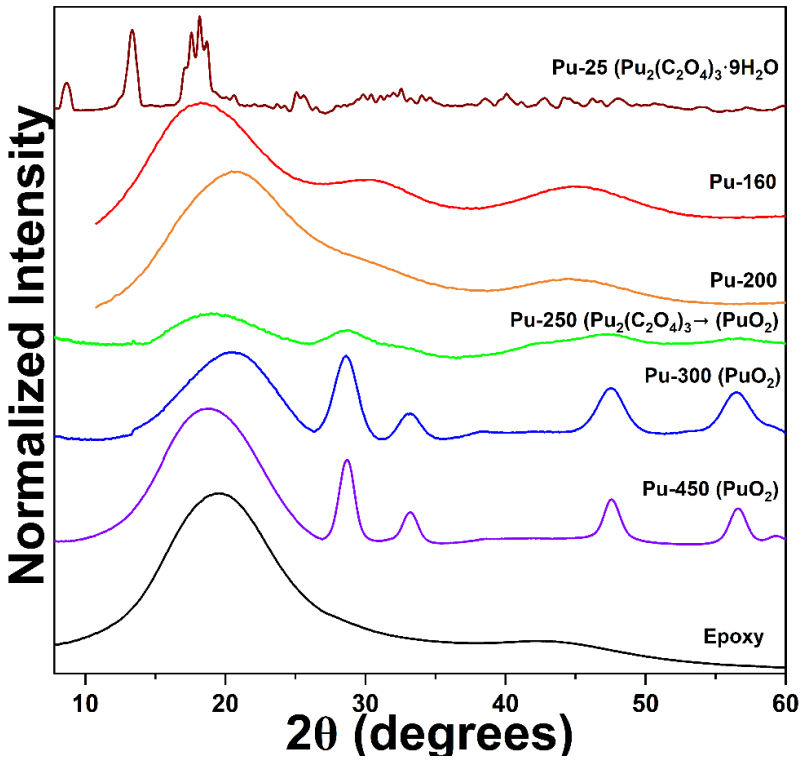

Fig. 1. Powder X-ray diffractograms of $Pu_2(C_2O_4)_3 \cdot 9H_2O$ produced at room temperature (**Pu-25**) and its degradation products as it is heated to 450 °C (**Pu-450**). Powder samples were encapsulated in an epoxy coating to provide protection from radiological hazards; the diffraction characteristics of the epoxy coating are provided for reference.

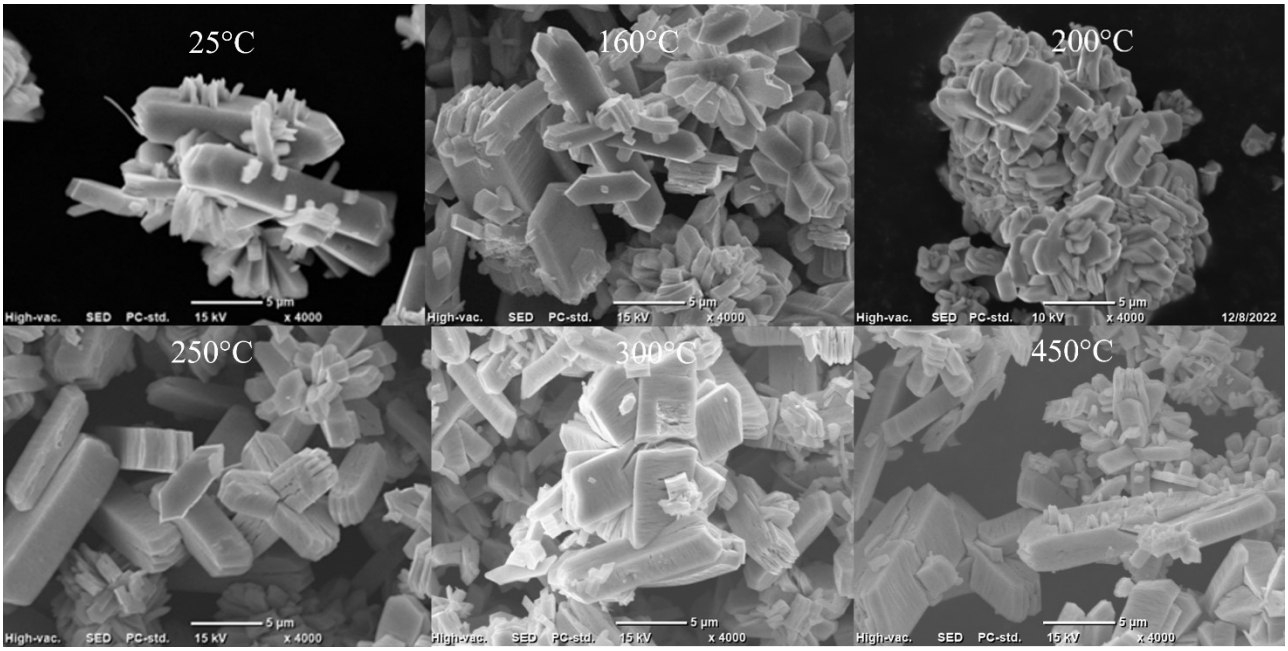

Fig. 2. Scanning electron micrographs of $Pu_2(C_2O_4)_3 \cdot 9H_2O$ (**Pu-25**) and its thermal degradation products under 4000x magnification.

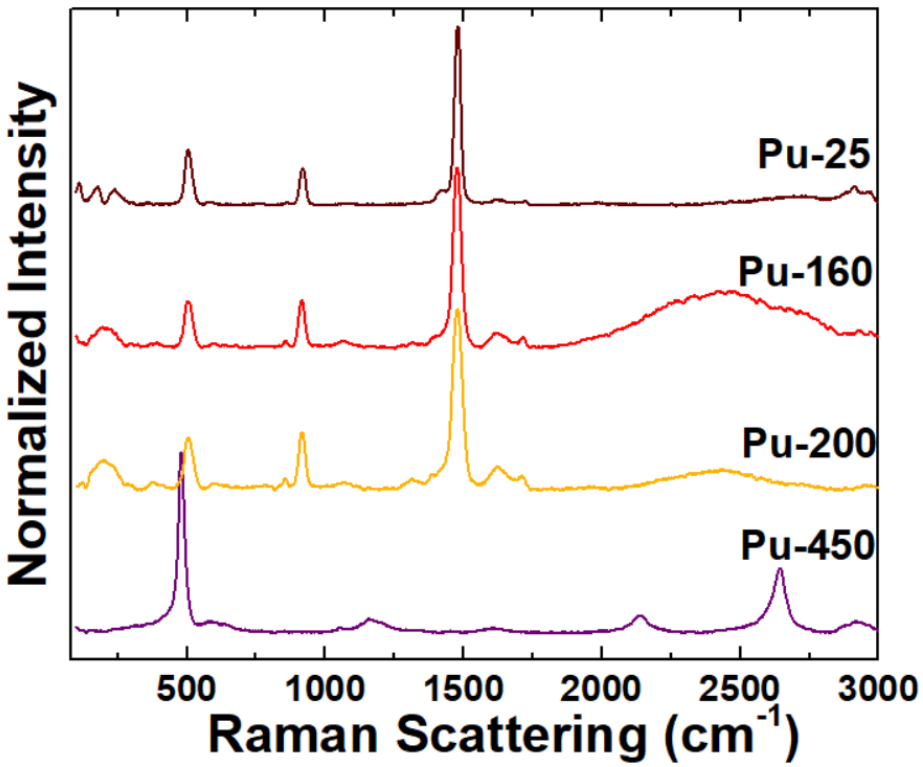

Fig. 3. Raman spectra of $Pu_2(C_2O_4)_3$•$9(H_2O)$ produced at room temperature (**Pu-25**) and its thermal degradation. Spectra at 250 ºC and 300 ºC are omitted because they contained significant fluorescence that overwhelmed the Raman signal (see Fig. S9)

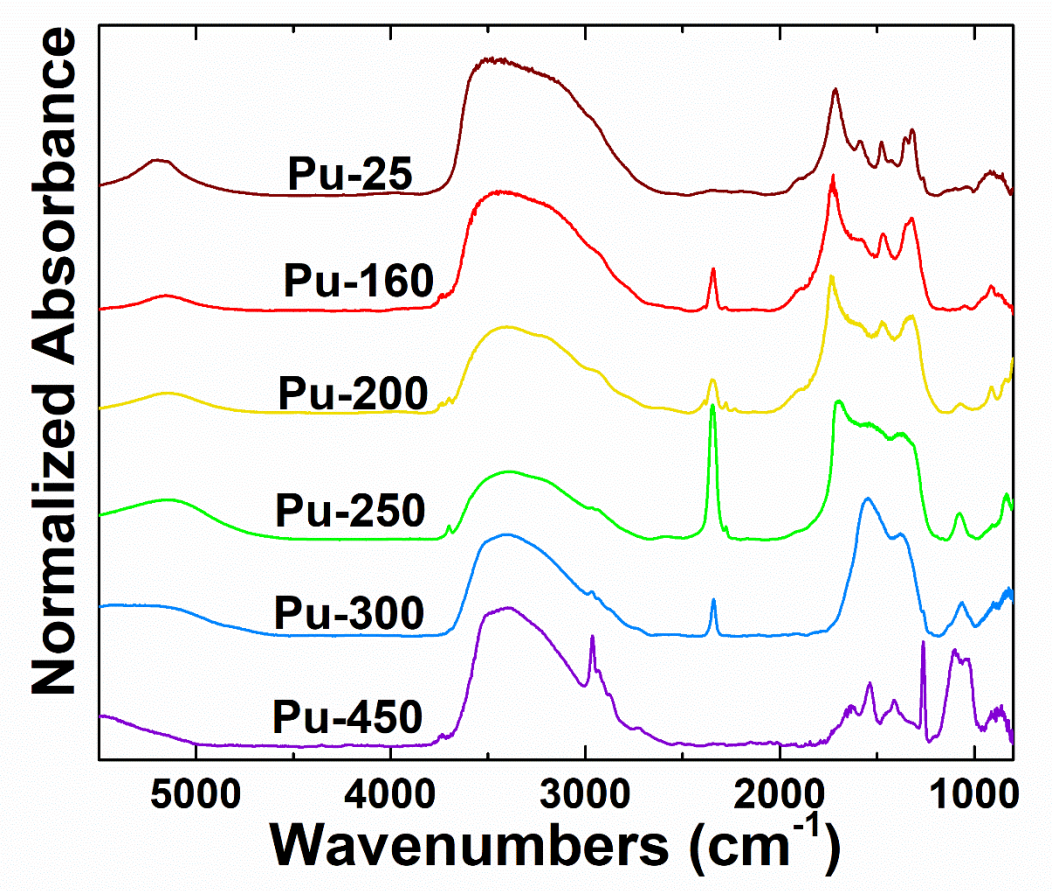

Fig. 4. IR spectra of $Pu_2(C_2O_4)_3$•9(H_2O) (**Pu-25**) and its thermal degradation products.